Dalton Transactions

ROYAL SOCIETY OF CHEMISTRY

PAPER

View Article Online
View Journal

Cite this: DOI: 10.1039/d5dt01873k

Remarkable coordination variability of the P,C,P-pincer ligand in organotin(IV) compounds – a promising outlook for other p-block elements

Richard Chlebík,[a] Erik Kertész,[b] Milan Erben,[a] Aleš Růžička,[a] Roman Jambor,[a] Zoltán Benkő *[b,c] and Libor Dostál *[a]

The coordination properties of the P,C,P-pincer ligand (**Ar** = 2,6-(tBu$_2$PO)$_2$C$_6$H$_3$) with organotin(IV) compounds were examined. For this purpose, a set of neutral compounds including ArSnPh$_2$Cl (**1**), ArSnPhCl$_2$ (**2**) and ArSnCl$_3$ (**3**), ArSnBu$_3$ (**4**) and the cations [ArSnPh$_2$][BArF] (**1$^+$[BArF]$^-$**), [ArSnPhCl][BArF] (**2$^+$[BArF]$^-$**), [ArSnCl$_2$][BArF] and (**3$^+$[BArF]$^-$**) ([BArF] = [3,5-(CF$_3$)$_2$C$_6$H$_3$]$_4$B) were prepared and characterized by multinuclear NMR spectroscopy and single-crystal (sc) X-ray diffraction analysis (**2**, **3**, **1$^+$[BArF]$^-$** and **3$^+$[BArF]$^-$**). This study revealed different types of ligand coordination, *i.e.* no P → Sn intramolecular interaction in **1** and **2**, while one P atom is coordinated in **3** and both P atoms in tin cations **1$^+$**, **2$^+$** and **3$^+$**. To further elucidate the strength of these P → Sn dative bonds, all compounds were reacted with [BH$_3$(SMe$_2$)] to prove whether it coordinates toward pendant P atoms or even de-coordinates those P atoms already connected to the tin atom. Thus, in **1**, **2**, and **4**, both P atoms formed complexes with the borane, while in **3** only one phosphorus reacted with BH$_3$, because the second remained bonded to the tin atom. Finally, even in the cation **1$^+$** one of the P atoms could be blocked by borane leaving the tin atom four-coordinated, while it was not possible for **2$^+$** and **3$^+$**. DFT calculations were used to gain a deeper insight into the P → Sn bonding interaction in the studied compounds.

Received 5th August 2025,
Accepted 5th September 2025

DOI: 10.1039/d5dt01873k

rsc.li/dalton

Introduction

Since their first appearance in the late seventies,[1] C-monoanionic Y,C,Y-pincers,[2] built-up as *ortho*, *ortho*-substituted phenyl rings (Y = neutral 2e donor atom, *e.g.* N, P, S, O *etc.*), have been developed into a prominent class of ligands that have found multifaceted applications with most metals across the periodic system. Their popularity stems mainly from their general applicability and high versatility in fine-tuning their coordination pocket, and steric and electronic properties (Fig. 1A), and the knowledge of these fascinating ligands is well established in the chemical community. When considering the donor atom Y, trivalent phosphorus immediately springs to mind as an excellent donor for most transition metals because its donating ability can be quite easily influenced. This has caused widespread utilization of P,C,P-ligands and it is undisputed that transition metal P,C,P-complexes constitute a large family of intriguing compounds with miscellaneous applications.[2,3]

In striking contrast, no complexes of p-block elements with classical P,C,P-ligands have been reported to the best of our knowledge so far. This is quite surprising due to the fact that various types of closely related N,C,N-, O,C,O- and O,C,N-ligands have been recognized as very useful structurally analogous platforms for p-block elements.[4] Examination of their coordination capabilities using organotin(IV) compounds as suitable model species has been a common feature in their introduction into the chemistry of main group elements. The first examples of N,C,N-tin(IV) complexes were reported by van Koten in 1989,[5] whereas the O,C,O-analogues were introduced by Jurkschat[6] (1988) and later on (2002) by our group[7] (Fig. 1B–D). Since these origins, the chemistry of all ligands has spread to other main group elements containing central atoms in various oxidation states and bonding situations. Consequently, interesting and relevant examples can be found with elements of Group 14,[8–10] 13,[11,12] 15 [13–15] and 16,[16] underlining the exceptional utility of these coordination platforms.

In the present contribution, we introduce for the first time the P,C,P-pincer ligand (**Ar** = 2,6-(tBu$_2$PO)$_2$C$_6$H$_3$, Fig. 1E),

[a]*Department of General and Inorganic Chemistry, University of Pardubice, Studentská 573, CZ 532 10 Pardubice, Czech Republic. E-mail: libor.dostal@upce.cz*
[b]*Department of Inorganic and Analytical Chemistry, Faculty of Chemical Technology and Biotechnology, Budapest University of Technology and Economics, Műegyetem rkp. 3, H-1111 Budapest, Hungary. E-mail: benko.zoltan@vbk.bme.hu*
[c]*HUN-REN-BME Computation Driven Chemistry Research Group, H-1111 BudapestMűegyetem rkp. 3, Hungary*

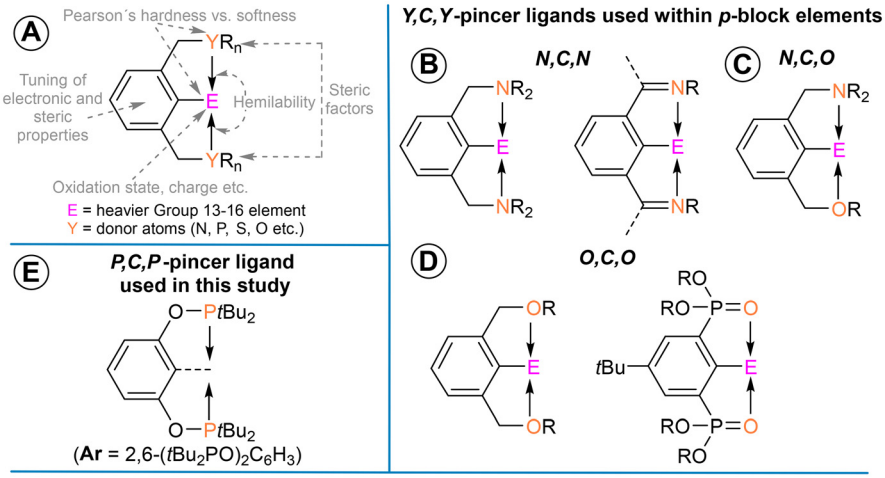

Fig. 1 General structure of Y,C,Y-pincer ligands considered in this study (A). Structurally related ligands used in the chemistry of p-block elements (B–D). The P,C,P-pincer ligand used in this study (E).

which is so successful in transition metal chemistry,[17] to the field of p-block elements. This study is aimed at validating a synthetic protocol based on the utilization of the lithiated precursor **ArLi** for the preparation of organotin(IV) compounds, while the tuning of the Lewis acidity of the central atom should allow us to obtain various coordination modes of the ligand. A complete set of both neutral and cationic tin compounds was synthesized and characterized for this purpose, while remarkable coordination variability of this ligand was obtained. The relative strength of intramolecular P → Sn interaction(s) was studied using multinuclear NMR spectroscopy in solution, single crystal (sc) X-ray diffraction analysis in the solid state and chemically by reacting isolated tin complexes with $[BH_3(SMe_2)]$ aiming to block/de-coordinate accessible phosphorus function(s). The obtained coordination modes are also compared with those of the closest analogues shown in Fig. 1B and D. A detailed DFT investigation was also performed to acquire deeper insight into the nature of P → Sn bonds in target compounds.

Results and discussion

Synthesis, NMR studies, and structures

The lithiation of the **ArBr** ligand precursor with *n*BuLi using the literature protocol[18] provided the organolithium complex $[2,6\text{-}(t\mathrm{Bu_2PO})_2C_6H_3]Li$ (**ArLi**), while its treatment with Ph_2SnCl_2, $PhSnCl_3$, and $SnCl_4$ in a 1 : 1 stoichiometric ratio gave the organotin(IV) compounds $ArSnPh_2Cl$ (**1**), $ArSnPhCl_2$ (**2**) and $ArSnCl_3$ (**3**) as colorless solids in reasonable yields (Scheme 1). In contrast, we were unable to isolate and crystallize a pure sample of the tetraorganotin(IV) counterpart $ArSnPh_3$ using the reaction between **ArLi** and Ph_3SnCl. Therefore, an analogous tetraorgano-type compound $ArSnBu_3$ (**4**) was synthesized (Scheme 2) and isolated as a colorless oil using the same synthetic strategy.

The ^1H and $^{13}C\{^1H\}$ NMR spectra in C_6D_6 revealed an expected set of signals for both ligand and phenyl moieties attached to the tin atoms in **1** and **2**. Signals found in the $^{31}P\{^1H\}$ NMR spectra of **1** (155.8 ppm) and **2** (160.6 ppm) are close to that of the starting **ArBr** (154.2 ppm, Table 1). The $^{119}Sn\{^1H\}$ NMR spectra exhibited one signal at −57.4/−44.7 ppm for **1**/**2**, respectively, both being only marginally shifted compared to signals for the related Ph_3SnCl (−48.0 ppm)[19] and Ph_2SnCl_2 (−32.0 ppm).[19] All these data suggest the absence of any significant intramolecular P → Sn interaction in benzene solution. Not surprisingly, the tin atom in the tetraorgano-derivative **4** also did not show any significant interaction with the phosphorus based on the obtained values of $\delta(^{31}P)$ = 154.0 ppm and $\delta(^{119}Sn)$ = −54.8 ppm.

Contrary to the NMR spectra for all the compounds mentioned above, the ^1H NMR spectrum of **3** in C_6D_6 showed two

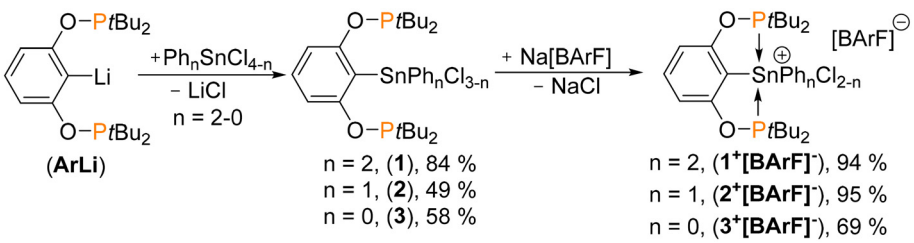

Scheme 1 Synthesis of the studied compounds. Note: [BArF] = $[3,5\text{-}(CF_3)_2C_6H_3]_4B$.

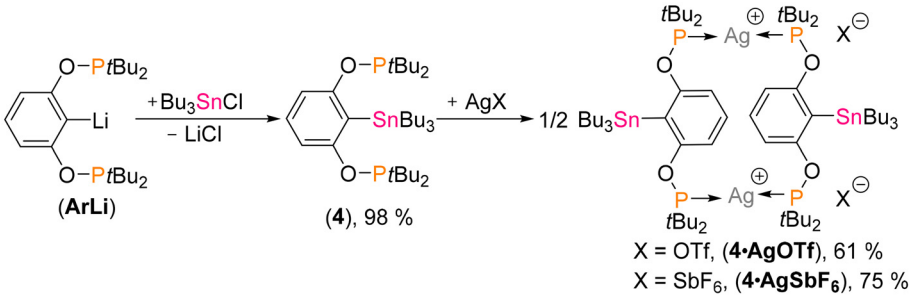

Scheme 2 Synthesis of complexes **4·AgOTf** and **4·AgSbF$_6$**.

Table 1 NMR data for the studied compounds. Selected $\delta(^{119}\text{Sn})$ and $\delta(^{31}\text{P})$ chemical shifts in ppm along with $^1J(^{119}\text{Sn}, ^{31}\text{P})$ and $^1J(^{109/107}\text{Ag}, ^{31}\text{P})$ coupling constants in Hz acquired in C_6D_6[a], $CDCl_3$[b] or CD_2Cl_2[c]. The relevant calculated chemical shifts at the PBE0/TZ2P(ZORA, spin–orbit)//ωB97X-D/def2-SVP and $^1J(^{119}\text{Sn}, ^{31}\text{P})$ coupling constants at the PBE0/TZ2P(ZORA, spin–orbit)//ωB97X-D/def2-TZVP level of theory are given in parentheses (note that the P centres are inequivalent in the computed structures and have only a minor difference)

	$\delta(^{119}\text{Sn})$	$\delta(^{31}\text{P})$	$^1J_{\text{Sn,P}}$		$\delta(^{119}\text{Sn})$	$\delta(^{31}\text{P})$	$^1J_{\text{Sn,P}}$
ArBr[a]	—	154.2 (154.2/154.5)	—	**2(BH$_3$)$_2$**[a]	−44.2 (−36.2)	159.6 (164.0/160.8)	—
ArBr(BH$_3$)[a]	—	155.6 (158.2)	—	**3**[a]	−274.1 (−298.5)	153.0/71.2[e] (150.3/51.0)	308 (888)
1[a]	−57.4 (−84.7)	155.8 (160.6/149.3)	—	**3**[b]	−275.0	153.9/72.0[e]	323
1[b,d]	−57.3 −203.4	157.3 150.5/83.4[e]	—	**3**$^+$**[BArF]**$^-$[f,f]	−194.0 (−210.6)	86.2 (71.5)	88 (342)
1$^+$**[BArF]**$^-$[c,f]	−187.6 (−227.7)	105.7 (105.6/88.7)	835 (843/829)	**3(BH$_3$)**[a]	−278.5 (−299.0)	152.8/70.6[e] (154.9/50.2)	211 (807)
1(BH$_3$)$_2$[a]	−57.4 (−79.8)	155.8 (159.3/155.8)	—	**4**[a]	−54.8	154.0	—
[1(BH$_3$)]$^+$ [BArF]$^-$[c,f]	−88.5 (−108.9)	156.0/116.2[e] (161.3/107.7)	285 (733)	**4(BH$_3$)$_2$**[a]	−46.7	154.5	—
2[a]	−44.7 (−24.5)	160.6 (151.6/162.0)	—	**4·AgOTf**[c]	−43.3	170.0	568/494[g]
2[b,d]	−45.7 −224.2[d]	160.6 151.6/77.1[e]	—	**4·AgSbF$_6$**[c]	−42.4	169.7	567/497[g]
2$^+$ **[BArF]**$^-$[c,f]	−214.4 (−240.3)	97.2 (83.4/83.3)	640 (702)				

[a] Acquired in C_6D_6. [b] Acquired in $CDCl_3$. [c] Acquired in CD_2Cl_2. [d] Two sets of signals for **1**/**1′**and **2**/**2′** detected. [e] Two signals detected. [f] The calculation was carried out without the counter anion. [g] For **4·AgOTf** and **4·AgSbF$_6$** the values correspond to $^1J(^{109/107}\text{Ag}, ^{31}\text{P})$.

signals for *t*Bu$_2$P groups and three signals for aromatic C*H* groups of the Ar ligand pointing to a non-equivalence of ligand arms. This is supported by the observation of six signals for aromatic carbon atoms in the $^{13}C\{^1H\}$ NMR spectrum. Furthermore, the $^{31}P\{^1H\}$ NMR spectrum contained two signals, one observed close to the value for **ArBr** (153.0 ppm), while the second is significantly high-field shifted (71.2 ppm) and flanked by tin satellites ($^1J(^{119/117}\text{Sn}, ^{31}\text{P})$ = 308 Hz). This resonance pattern indicates tight coordination of the single ligand arm to the central tin atom, while the second phosphorus function remains pendant. This finding is further corroborated by the detection of a doublet at −274.1 ppm ($^1J(^{119}\text{Sn}, ^{31}\text{P})$ = 308 Hz) in the corresponding $^{119}Sn\{^1H\}$ NMR spectrum. In particular, the latter value indicates a tin atom more shielded compared to that in $PhSnCl_3$ (*cf.* −63 ppm),[19] which is consistent with coordination of phosphorus with tin.

Furthermore, to elucidate a plausible influence of the solvent, ^1H, $^{31}P\{^1H\}$ and $^{119}Sn\{^1H\}$ NMR spectra of **1**–**3** in $CDCl_3$ were recorded as well. The ^1H NMR spectra in all cases revealed a set of broad signals. The $^{31}P\{^1H\}$ spectrum of **3** again revealed two signals at 153.9 and 72.0 ppm, where the latter is flanked by tin satellites ($^1J(^{119/117}\text{Sn}, ^{31}\text{P})$ = 323 Hz), while one doublet is obtained in the $^{119}Sn\{^1H\}$ NMR spectrum at −275.0 ppm ($^1J(^{119/117}\text{Sn}, ^{31}\text{P})$ = 323 Hz). These data are almost identical to those found in C_6D_6 proving that the same structure for **3** exists in both solvents (Fig. 2A). Surprisingly, two sets of signals were observed in the $^{31}P\{^1H\}$ and $^{119}Sn\{^1H\}$ NMR spectra in $CDCl_3$ for **1** and **2**. The values of the major set are again closely related to the data described above in C_6D_6, *i.e.* one signal in the $^{31}P\{^1H\}$ NMR spectra at 157.3 (for **1**) and 160.6 ppm (for **2**) and one singlet in the $^{119}Sn\{^1H\}$ NMR spectra at −57.3 (for **1**) and −45.7 ppm (for **2**). However, the minor set of signals is indicative of the presence of second isomers **1′** and **2′** with one coordinated P donor group similar to the situation found in **3**. Thus, the $^{31}P\{^1H\}$ NMR spectra consist of two broad signals at 150.5/83.4 ppm and 151.6/77.1 ppm for **1′**/**2′**, respectively. Importantly, the $^{119}Sn\{^1H\}$ NMR spectra revealed a second signal in addition to that of **1** and **2** at −203.4 for **1′** and −224.2 ppm for **2′** (*cf.* −274.1 ppm for **3**, Fig. 2B and C). In conclusion, whereas compound **3** exhi-

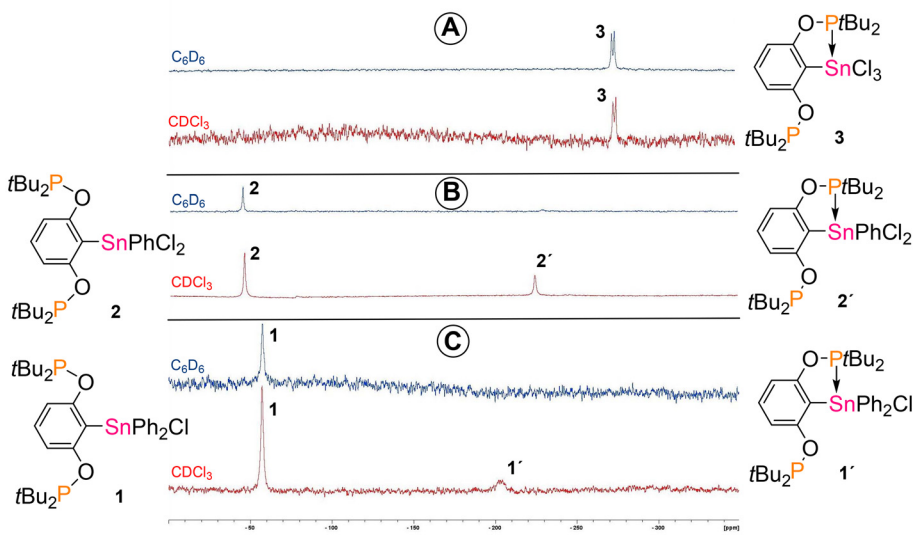

Fig. 2 Comparison of $^{119}Sn\{^1H\}$ NMR spectra of **1–3** acquired in C_6D_6 (blue) or $CDCl_3$ (red) showing the same structure for **1** (A) and plausible formation of isomers **1′** (B) and **2′** (C) in $CDCl_3$.

bits the same structure with one coordinated P-donor in both C_6D_6 and $CDCl_3$, compounds **1** and **2** show no tightly rigid coordination of P atoms in C_6D_6, but two isomers, *i.e.* **1**/**1′** and **2**/**2′**, most probably coexist in $CDCl_3$ solution.

The molecular structures of **2** and **3** determined by sc-XRD analysis are shown in Fig. 3 and are consistent with the proposed structures in C_6D_6 solution above. The Sn(1) atom lacks any close interaction with phosphorus donor atoms in **2** according to the Sn(1)–P(1/2) distances 4.8286(7)/4.7695(10) Å, respectively, while adopting a distorted tetrahedral geometry. The C(1)–Sn(1)–C(23) angle (128.86(8)°) represents the main deviation from the ideal shape. In sharp contrast, a strong Sn(1)–P(1) interaction (2.6313(9) Å, *cf.* $\sum_{cov}$(P,Sn) = 2.51 Å (ref. 20)) is observed in **3** leaving the P(2) atom pendant (Sn(1)–P(2) 4.9105(11) Å). This leads to a distorted trigonal bipyramidal array around the Sn(1) atom (τ = 0.77;[21] note: τ = 0 for ideal square pyramid geometry and τ = 1 for ideal trigonal bipyramid geometry) with C(1) and Cl(3) located at the apex positions (*cf.* C(1)–Sn(1)–Cl(3) 165.67(8)°).

The coordination behavior of the P,C,P-ligand in **1–3** deserves attention when compared to the previously reported N,C,N- and O,C,O-ligand counterparts (Fig. 3). No significant intramolecular P → Sn interaction was detected in **1** (in C_6D_6 solution based on NMR) and **2** (in C_6D_6 solution based on NMR and in the solid state based on sc-XRD) whereas in the N,C,N-chelated analogues $[(2,6\text{-}(Me_2NCH_2)_2C_6H_3)SnPh_2]^+$ (**A1**$^+$)[22] and $[2,6\text{-}(Me_2NCH_2)_2C_6H_3]SnPhCl_2$ (**A2**)[23] both nitrogen atoms coordinate the tin atom quite tightly, which even results in autoionization of the former allowing isolation of the whole set of tin cations related to **A1**$^+$ with various counter anions.[9l] In the case of $[2,6\text{-}(MeOCH_2)_2C_6H_3]SnPh_2Cl$ (**B1**) and $[2,6\text{-}(MeOCH_2)_2C_6H_3]SnPhCl_2$ (**B2**),[7] the oxygen atoms are, albeit weakly, coordinated to the central atom as well. Similar autoionization (as in **A1**$^+$) followed by elimination of an alkyl halide led to the isolation of a neutral compound $[2\text{-}(OP(O)(OEt))\text{-}4\text{-}t\text{Bu-}6\text{-}(P(O)(OEt)_2)C_6H_2]SnPh_2$ (**C1**)[24] in the case of Jurkschat's O,C,O-ligand (Fig. 3), while both oxygen atoms are coordinated in the diorgano-compound $[2,6\text{-}(P(O)(OEt)_2)_2\text{-}4\text{-}t\text{Bu-}C_6H_2]SnPhCl_2$ (**C2**) leading to a distorted octahedral geometry.[6] Mono-organotin compounds $[2,6\text{-}(Me_2NCH_2)_2C_6H_3]SnBr_3$ (**A3**), $[2,6\text{-}(MeOCH_2)_2C_6H_3]SnCl_3$ (**B3**) and $[2,6\text{-}(P(O)(OEt)_2)_2\text{-}4\text{-}t\text{Bu-}C_6H_2]SnCl_3$ (**C3**) again have both donor atoms coordinated with the tin atom giving an octahedral array around the tin atom, but the pincer ligand adopts either a pseudo-meridional (**A3**[9k] and **C3**[24]) or a pseudo-facial (**B3**[7]) coordination mode. In contrast, in the case of **3**, only one of the P atoms is sufficient for stabilization of the $SnCl_3$ unit, while the second phosphorus remains pendant as proven both in solution (NMR) and in the solid state (sc-XRD). This results in a distorted trigonal bipyramidal array around the tin atom in **3** and underlines promising potential of the ligand to stabilize highly Lewis acidic species (*vide infra*).

To enforce the obviously accessible intramolecular P → Sn interaction(s) (as found in **3**), **1** was reacted with 1 eq. of $AgSbF_6$ aimed at the production of the corresponding organotin cation $[ArSnPh_2][SbF_6]$ (**I**, Fig. 4). However, *in situ* inspection of the reaction mixture by $^{31}P\{^1H\}$ NMR spectroscopy showed the formation of three species (Fig. 4), which is evidently the result of a high Ag^+ ion affinity toward the phosphorus donors that hampered a clean abstraction of the chloride from the tin center. The target cation **I** revealed only one signal at $\delta(^{31}P)$ = 105.8 ppm ($^1J(^{119/117}Sn,^{31}P)$ = 819 Hz), which is highly comparable with that of the subsequently isolated cationic pair **1**$^+$**[BArF]**$^-$ (*cf.* $\delta(^{31}P)$ = 105.7 ppm, $^1J(^{119/117}Sn,^{31}P)$ = 835 Hz, *vide infra*). The second species was tentatively assigned to a complex of **I** with incipient AgCl, *i.e.* compound **II** (Fig. 4), exhibiting two (1 : 1) signals. The first signal, attributed to the phosphorus atom coordinated to tin, resonated at

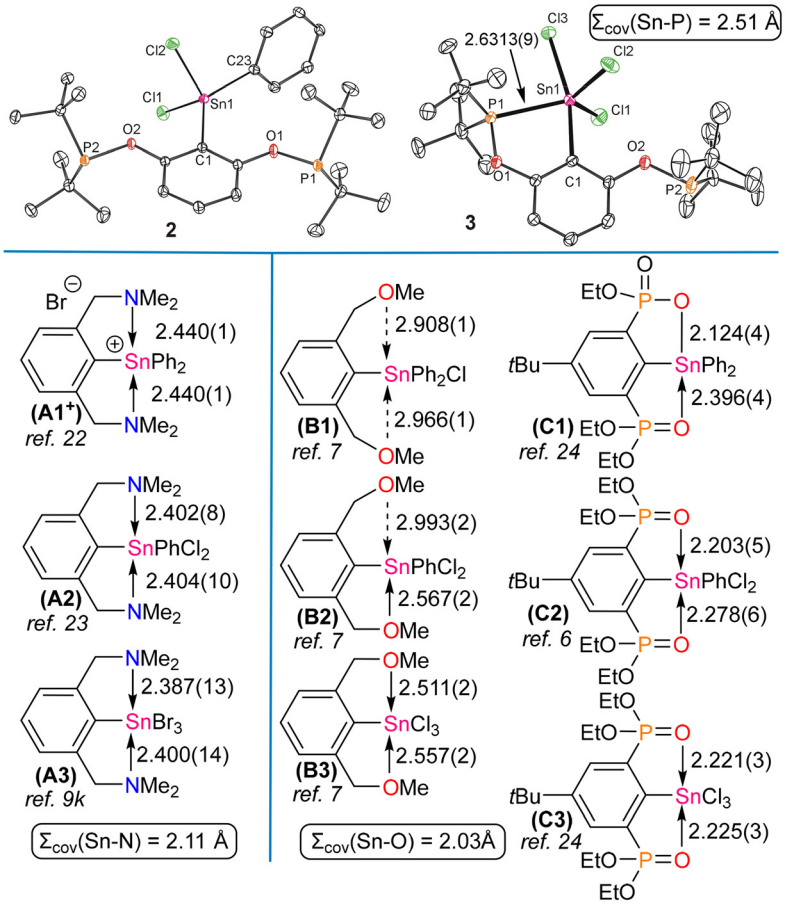

Fig. 3 ORTEP drawings of molecular structures of **2** (top-left) and **3** (top-right). The thermal ellipsoids are given with 30% probability and hydrogen atoms are omitted for clarity. Selected structural parameters for **2**: C(1)–Sn(1) 2.109(2), C(23)–Sn(1) 2.114(2), Cl(1)–Sn(1) 2.3466(8), Cl(2)–Sn(1) 2.3401 (8), P(1)–Sn(1) 4.8286(7), and P(2)–Sn(1) 4.7695(10) Å. For **3**: C(1)–Sn(1) 2.163(3), Cl(1)–Sn(1) 2.3360(11), Cl(2)–Sn(1) 2.3521(11), Cl(3)–Sn(1) 2.4195(11), P(1)–Sn(1) 2.6313(9), and P(2)–Sn(1) 4.9105(11) Å; C(1)–Sn(1)–Cl(3) 165.67(8)°. Comparison with N,C,N- and O,C,O-chelated analogues (below). Please note that when the structure of organotin chlorides is not reported, the closest analogues are used (*i.e.*, in the case of **A1**$^+$ and **A3**).

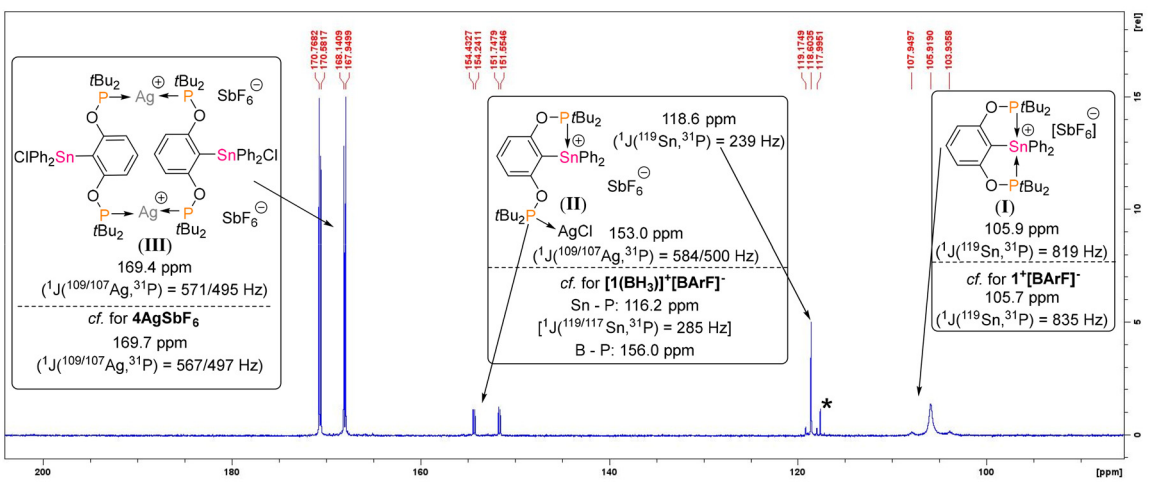

Fig. 4 $^{31}P\{^1H\}$ NMR spectrum showing the reaction mixture after addition of $AgSbF_6$ to compound **1**. *Denotes unknown minor species.

$\delta(^{31}P)$ = 118.6 ppm ($^{1}J(^{119/117}Sn,^{31}P)$ = 239 Hz), closely resembling the value found for the ionic compound **[1(BH$_3$)]$^+$[BArF]$^-$**, where again only one phosphorus coordinates to the tin center (*cf.* $\delta(^{31}P)$ = 116.2 ppm, $^{1}J(^{119/117}Sn,^{31}P)$ = 285 Hz, *vide infra*). The second signal at $\delta(^{31}P)$ = 153.0 ppm was formed as a doublet of doublets, indicating a clear interaction with the silver atom as proven by $^{1}J(^{109/107}Ag,^{31}P)$ = 584/500 Hz. Finally, the most intense signal in the mixture was tentatively assigned to a simple donor–acceptor complex of **1** with $AgSbF_6$, *i.e.* {μ-(P,P)-Ag-[2,6-(tBu$_2$PO)$_2$C$_6$H$_3$]SnPh$_2$Cl}$_2$(SbF$_6$)$_2$ (**III**), observed as a doublet of doublets at 169.4 ppm ($^{1}J(^{109/107}Ag,^{31}P)$ = 571/495 Hz). To prove the proposed structure of the major product **III**, compound **4** lacking any chlorine available for the formation of AgCl, but containing pendant phosphorus donors at the same time, was treated with AgX (X = OTf or SbF_6). In fact, this reaction readily provided the expected complexes {μ-(P,P)-Ag-[2,6-(tBu$_2$PO)$_2$C$_6$H$_3$]SnBu$_3$}$_2$(X)$_2$ (X = OTf or SbF_6), *i.e.* **4·AgOTf** and **4·AgSbF$_6$**, according to Scheme 2 as direct analogues of proposed complex **III**.

Both compounds revealed a set of expected signals in their ^{1}H and $^{13}C\{^{1}H\}$ NMR spectra. The $^{119}Sn\{^{1}H\}$ NMR spectra showed one signal at −43.3/−42.3 ppm for **4·AgOTf**/**4·AgSbF$_6$**, respectively, close to that of the starting **4**, whereas the $^{31}P\{^{1}H\}$ NMR spectrum contained a doublet of doublets for each complex at 170.0/169.7 ppm ($^{1}J(^{109/107}Ag,^{31}P)$ = 568/494 Hz for **4·AgOTf**, $^{1}J(^{109/107}Ag,^{31}P)$ = 567/497 Hz for **4·AgSbF$_6$**) almost identical to that of complex **III**. Finally, the molecular structures of both complexes were established by sc-XRD analysis for **4·AgOTf** (Fig. 5) (Fig. S89 for **4·AgSbF$_6$**) and structurally they are closely related, thus only that of **4·AgOTf** is described in more detail. The triflate anions are located outside the coordination sphere of silver atoms, while these are coordinated by two phosphorus from two different ligands, leading to a centrosymmetric dimeric dication (Fig. 5). The Ag(1)–P(1/2) bond lengths of 2.4044(4)/2.4017(4) Å correspond closely to the

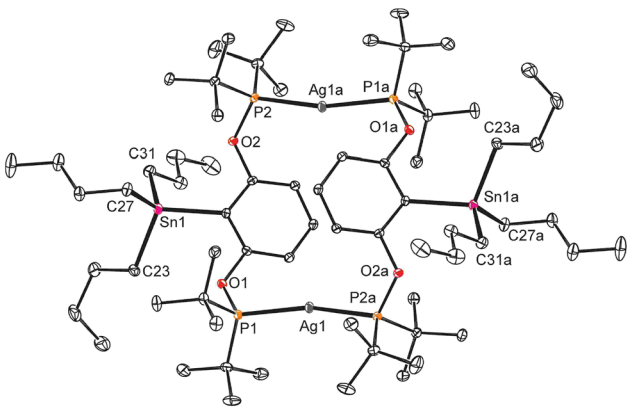

Fig. 5 ORTEP drawing of molecular structures of **4·AgOTf**. The thermal ellipsoids are given with 30% probability, and hydrogen atoms and the OTf anions are omitted for clarity. Selected structural parameters: C(1)–Sn(1) 2.1799(13), C(23)–Sn(1) 2.1572(15), C(27)–Sn(1) 2.1597(18), C(31)–Sn(1) 2.1658(16), Ag(1)–P(1) 2.4044(4), and Ag(1)–P(2a) 2.4017(4) Å; P(1)–Ag(1)–P(2a) 166.05(2)°.

$\sum_{cov}$(P,Ag) = 2.39 Å (ref. 20) while the P(1)–Ag(1)–P(2a) bonding angle is 166.05(2)°. The organotin fragments are directed away from the center of the molecule, and tin atoms adopt a distorted tetrahedral coordination geometry.

The utilization of a low-nucleophilic anion silver salt for the abstraction of the chloride from **1** turned out to be non-selective and complicated due to the formation of a P–Ag complex, therefore the sodium salt Na[BArF] ([BArF] = [3,5-(CF$_3$)$_2$C$_6$H$_3$]$_4$B) was used where significantly lower tendency of sodium ions to complex with pendant phosphorus atoms was expected. Indeed, this approach allowed smooth isolation of a full set of organotin(IV) cations (Scheme 1), *i.e.* [ArSnPh$_2$][BArF] (**1$^+$[BArF]$^-$**), [ArSnPhCl][BArF] (**2$^+$[BArF]$^-$**) and [ArSnCl$_2$][BArF] (**3$^+$[BArF]$^-$**), as crystalline solids in quantitative yields. The ^{1}H and $^{13}C\{^{1}H\}$ NMR spectra in CD_2Cl_2 contained anticipated sets of signals for the ligand, phenyl moieties as well as for the [BArF]$^-$ anion for these compounds. The presence of the [BArF]$^-$ anion was also corroborated by $^{11}B\{^{1}H\}$ (signal at −7 ppm) and $^{19}F\{^{1}H\}$ (signal at −62.8 ppm) NMR spectra. The $^{31}P\{^{1}H\}$ NMR spectra revealed one signal for **1$^+$**/**2$^+$** at 105.7/97.2 ppm, both being significantly high-field shifted compared to starting **1** and **2** (Table 1). **3$^+$** showed a signal at 86.2 ppm, indicating symmetric coordination of both donor atoms of the pincer ligand resembling the chemical shift value of the coordinated phosphorus atom in **3** (Table 1). $^{119}Sn\{^{1}H\}$ NMR signals were detected as triplets for **1$^+$**/**2$^+$** at −187.6/−214.4 ppm and these are high-field shifted compared to those for **1** and **2**, indicating that both phosphorus atoms are coordinated to the central tin atom, unlike the neutral species, also leading to an increase in the coordination number of the tin atom to five (Table 1). In contrast, the chemical shift value of −194.0 ppm observed for **3$^+$** is low-field shifted compared to that for **3** (−274.1 ppm). This finding probably reflects two contradictory factors that influence the shielding of tin in **3$^+$**, *i.e.* the positive charge on the central atom *vs.* the coordination of the second phosphorus atom, while the tin atom formally preserves its 5-fold coordination similarly to **3**. A clear trend is also found among values of $^{1}J(^{119/117}Sn,^{31}P)$ that amount to 835/640/88 Hz for **1$^+$**/**2$^+$**/**3$^+$**, respectively, *i.e.* becoming lower with increasing relative strength of the P → Sn interaction.

The structures of cations **1$^+$** and **3$^+$** are depicted in Fig. 6, but all attempts to determine the structure of **2$^+$** resulted in heavily disordered structures only. The anions are situated outside the metal coordination sphere. The tin atom is tightly coordinated in both cationic parts by phosphorus atoms with the bond lengths Sn(1)–P(1)/(2) of 2.808(3)/2.7606(18) Å and 2.6689(7)/2.6647(7) Å for **1$^+$**/**3$^+$**, respectively. The shorter distances detected in **3$^+$** reflect the presence of a more Lewis acidic center (*cf.* $\sum_{cov}$(P,Sn) = 2.51 Å (ref. 20)). The obtained values are still longer than in related highly Lewis acidic tin(IV) compounds, such as [SnMe$_3$(PMe$_3$)]$^+$[AlCl$_4$]$^-$ (2.5861(9) Å)[25], [SnCl$_3$(OTf)(PMe$_3$)$_2$] (2.5496(9)/2.5506(9) Å)[26] or chelates [SnBu$_2$Cl(Me$_2$P(CH$_2$)$_2$PMe$_2$)]$^+$[AlCl$_4$]$^-$ (2.5696(8)/2.7601(8) Å) and [SnBu$_2$(Me$_2$P(CH$_2$)$_2$PMe$_2$)]$^{2+}${[AlCl$_4$]$^-$}$_2$ (2.5654(9)/2.521(9) Å).[25]

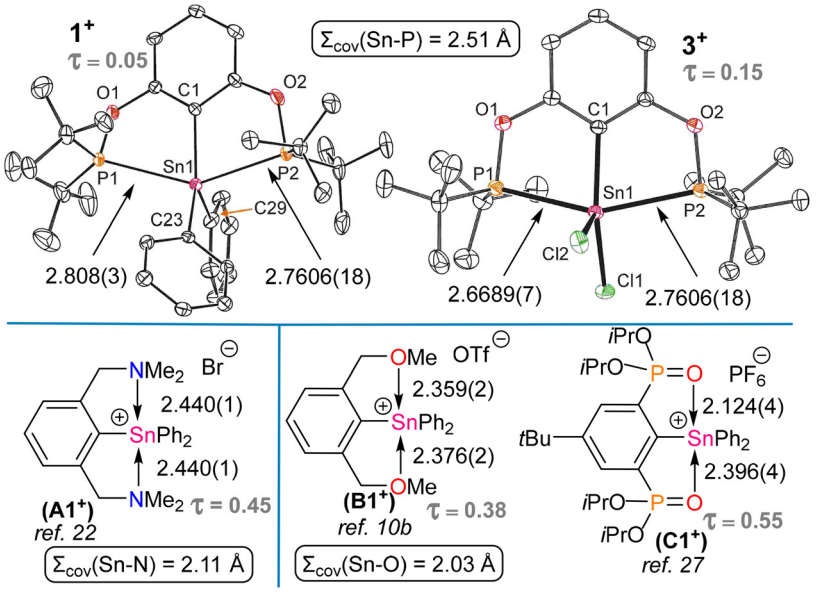

Fig. 6 ORTEP drawings of structures of $\mathbf{1}^+$ (top-left) and $\mathbf{3}^+$ (top-right). The thermal ellipsoids are given with 30% probability, and hydrogen atoms and $[BArF]^-$ anions are omitted for clarity. Selected structural parameters for $\mathbf{1}^+$: C(1)–Sn(1) 2.142(6), C(23)–Sn(1) 2.158(4), C(29)–Sn(1) 2.145(4), P(1)–Sn(1) 2.808(3), and P(2)–Sn(1) 2.7606(18) Å. For $\mathbf{3}^+$: C(1)–Sn(1) 2.128(2), Cl(1)–Sn(1) 2.3251(7), Cl(2)–Sn(1) 2.3217(7), P(1)–Sn(1) 2.6689(7), and P(2)–Sn(1) 2.6647(7) Å. Comparison with N,C,N- and O,C,O-chelated analogues $\mathbf{A1}^+$, $\mathbf{B1}^+$ and $\mathbf{C1}^+$ (below).

The coordination polyhedron is described in both cases as only slightly distorted square-pyramid with the C(29) and Cl(2) atoms in the apical position with τ = 0.05/0.15[21] for $\mathbf{1}^+/\mathbf{3}^+$, respectively.

Some analogues of $\mathbf{1}^+$ containing both N,C,N-, *i.e.* $[(2,6\text{-}(Me_2NCH_2)_2C_6H_3)SnPh_2]^+$ $(\mathbf{A1}^+)$[22] and O,C,O-ligands, *i.e.* $[(2,6\text{-}(MeOCH_2)_2C_6H_3)SnPh_2]^+$ $(\mathbf{B1}^+)$[10b] and $[(2,6\text{-}(P(O)(OiPr)_2)_2\text{-}4\text{-}t\text{Bu-}C_6H_2)SnPh_2]^+$ $(\mathbf{C1}^+)$[27] were structurally characterized showing two strong intramolecular interactions with donor atoms (Fig. 6), while the coordination polyhedron is somewhat more distorted in direction toward the trigonal bipyramid according to the τ [21] value (*cf.* 0.45/0.38/0.55 for $\mathbf{A1}^+/\mathbf{B1}^+/\mathbf{C1}^+$, respectively *vs.* 0.05 in $\mathbf{1}^+$). $\mathbf{3}^+$ containing $[ArSnCl_2]^+$ (τ = 0.15) represents, to the best of our knowledge, the first example of such an organotin pincer cation reported to date.

The square-pyramidal arrangement in the solid state structures of $\mathbf{1}^+$ and $\mathbf{3}^+$ can be traced back to the presence of bulky *t*Bu groups at the P centers. According to DFT calculations, the model analogues with methyl substituents instead of *t*Bu reveal a significant increase in the τ parameters to 0.48/0.55 for the two hypothetical cations $\mathbf{1}^+\mathbf{(Me)}/\mathbf{3}^+\mathbf{(Me)}$, respectively, thus more resembling their N,C,N- and O,C,O-ligand counterparts. Note that the optimized geometries of the original $\mathbf{1}^+/\mathbf{3}^+$ cations are highly similar to the solid-state structures with τ = 0.01/0.19, respectively.

To further experimentally elucidate the strength of the P → Sn interaction(s) in the studied compounds, all were treated with $[BH_3(SMe_2)]$ to determine whether they coordinate with the phosphorus donor atom(s). Not surprisingly, in the case of **ArBr** (taken as a model) and compounds **1**, **2** and **4**, both phosphorus atoms are smoothly coordinated toward the borane as no significant P → Sn interaction was observed in the parent compounds (Scheme 3). Thus, the compounds $\mathbf{ArBr(BH_3)_2}$, $\mathbf{1(BH_3)_2}$, $\mathbf{2(BH_3)_2}$ and $\mathbf{4(BH_3)_2}$ could be isolated and characterized using multinuclear NMR spectroscopy (see the SI) and sc-

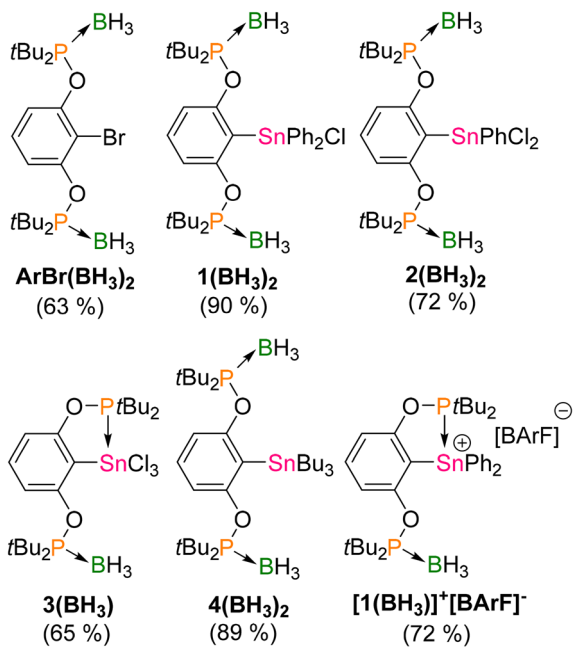

Scheme 3 Structures of isolated borane adducts obtained by reaction of parent compounds with 2 eq. of $[BH_3(SMe_2)]$, along with isolated yields given in parentheses. Note: [BArF] = $[3,5\text{-}(CF_3)_2C_6H_3]_4B$.

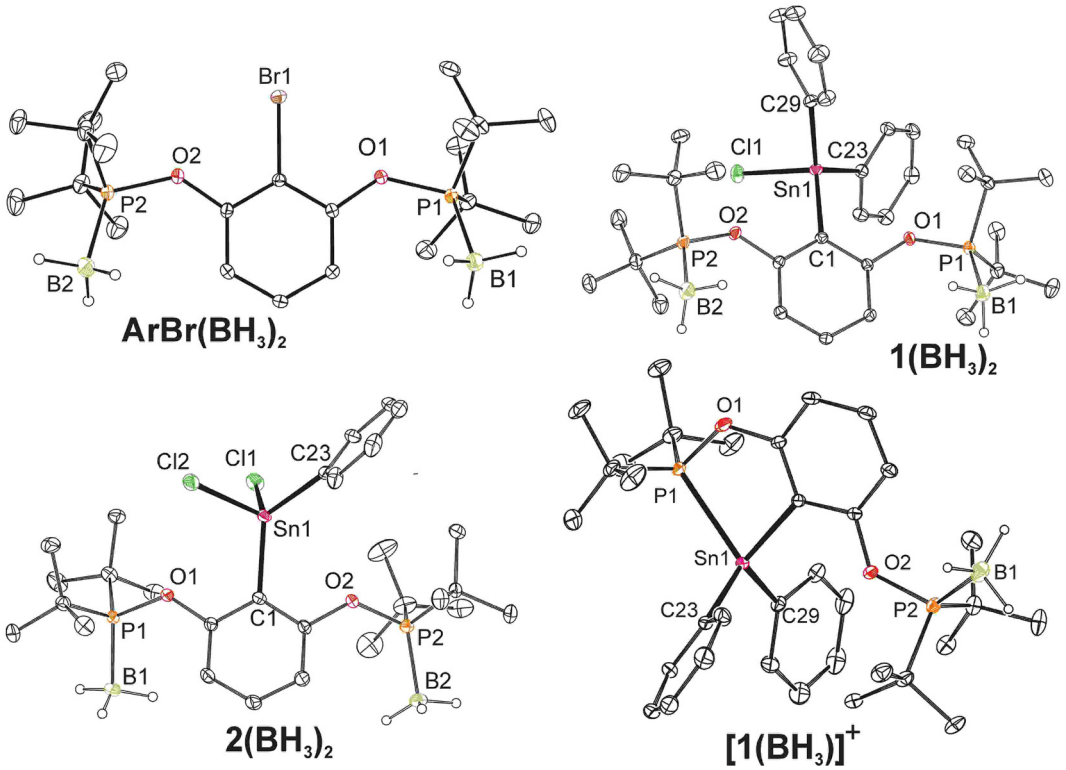

Fig. 7 ORTEP drawings of molecular structures of **ArBr(BH$_3$)$_2$**, **1(BH$_3$)$_2$**, **2(BH$_3$)$_2$** and **[1(BH$_3$)]$^+$**. The thermal ellipsoids are given with 30% probability, and hydrogen atoms (except in BH$_3$ groups) and the [BArF]$^-$ anion are omitted for clarity. Selected structural parameters for **ArBr(BH$_3$)$_2$**: B(1)–P(1) 1.9244(17) and B(2)–P(2) 1.918(2) Å. For **1(BH$_3$)$_2$**: C(1)–Sn(1) 2.1330(18), C(23)–Sn(1) 2.125(2), C(29)–Sn(1) 2.122(2), Cl(1)–Sn(1) 2.3772(7), B(1)–P(1) 1.922(3), and B(2)–P(2) 1.926(2) Å. For **2(BH$_3$)$_2$**: C(1)–Sn(1) 2.1147(17), C(23)–Sn(1) 2.1102(19), Cl(1)–Sn(1) 2.3297(5), Cl(2)–Sn(1) 2.3491(6), B(1)–P(1) 1.919(2), and B(2)–P(2) 1.923(3) Å. For **[1(BH$_3$)]$^+$**: C(1)–Sn(1) 2.120(3), C(23)–Sn(1) 2.121(4), C(29)–Sn(1) 2.120(4), P(1)–Sn(1) 2.5825(6), and B(1)–P(2) 1.917(5) Å.

XRD analysis in the case of **ArBr(BH$_3$)$_2$**, **1(BH$_3$)$_2$** and **2(BH$_3$)$_2$** (Fig. 7).

In the case of **3**, only one of the phosphorus atoms could be blocked by BH_3 giving complex **3(BH$_3$)**, while using an excess of borane did not alter the result of the reaction. This fact is reflected by the observation of three signals for aromatic C*H* groups of the Ar ligand in the ^{1}H NMR spectrum pointing to a non-equivalence of ligand arms. Furthermore, two signals were detected in the $^{31}P\{^1H\}$ NMR spectrum, *i.e.* for the phosphorus atom bound to the tin atom at 70.6 ppm ($^1J(^{119/117}Sn,^{31}P)$ = 211 Hz) and for the second one at 152.8 ppm, which is broadened due to the coupling with boron nuclei. The $^{11}B\{^1H\}$ NMR spectrum revealed a signal at −37.8 ppm for the coordinated BH_3. The value of $\delta(^{119}Sn)$ = −278.5 ppm is only marginally shifted compared to that for **3** (*cf.* −274.1 ppm) indicating that the tin atom retains its coordination number of five as in the parent compound.

Treatment of **1$^+$[BArF]$^-$** with [BH_3(SMe$_2$)] quite surprisingly also gave a 1 : 1 complex with BH_3, *i.e.* **[1(BH$_3$)]$^+$[BArF]$^-$**, despite the fact that both phosphorus atoms were quite tightly coordinated to the tin atom in the starting compound. In contrast, no reaction was obtained for **2$^+$[BArF]$^-$** and **3$^+$[BArF]$^-$** reflecting the presence of more Lewis acidic tin centers that prevent de-coordination of phosphorus donor atoms from the metal center (*vide infra*). The ^{1}H and $^{13}C\{^1H\}$ NMR spectra of the cation **[1(BH$_3$)]$^+$** proved the nonequivalence of both ligand arms. The $^{31}P\{^1H\}$ NMR spectrum contained two signals: one at 116.2 ppm ($^1J(^{119/117}Sn,^{31}P)$ = 285 Hz) and the second at 156.0 ppm and, similarly, two signals were detected in the $^{11}B\{^1H\}$ NMR spectrum for the [BArF]$^-$ anion at −7.2 ppm and for the coordinated BH_3 at −40.1 ppm. The signal for the tin atom in **[1(BH$_3$)]$^+$** at −88.5 ppm is low-field shifted compared to that for the parent **1$^+$** (−187.6 ppm), reflecting the absence of one of the phosphorus donors in the tin coordination sphere after being blocked by the borane. The molecular structure is shown in Fig. 7 and, as expected, the P(2) is coordinated by the borane unit (P(2)–B(1) 1.917(5) Å). The P(2)–Sn(1) bond length is very short at 2.5825(9) Å, approaching the value of $\sum_{cov}$(P,Sn) = 2.51 Å (ref. 20) and, not only is it shorter than that in **1$^+$**, it is even shorter than the bond length in the above described cation **3$^+$**. It is also comparable to the value found in [SnMe$_3$(PMe$_3$)]$^+$[AlCl$_4$]$^-$ (2.5861(9) Å).[25] This evidently results only from the four-coordinated tin cation that adopts a distorted tetrahedral geometry in **[1(BH$_3$)]$^+$**.

Theoretical studies

To gain insight into the role of the P → Sn interaction on the stability of the P,C,P-chelate complexes, geometry optimization

and frequency calculations were performed using the ωB97X-D functional combined with the def2-SVP and def2-TZVP basis sets, which include pseudopotentials for Sn to account for relativistic effects. The same level of theory was applied successfully to describe the bonding of similar complexes previously.[28] The Polarizable Continuum Model (PCM) for benzene and dichloromethane was also employed to check the effect of the solvent on the optimized geometries, which proved to be negligible. On the optimized geometries, Natural Bond Orbital (NBO) analysis was carried out. Furthermore, to estimate the covalent character of the bonding interactions, Wiberg Bond Indices (WBI) and Mayer Bond Orders (MBO) were also calculated to complement the characteristic bond distances (Tables S2–S8). Since these bond orders give similar values, in the following, we will discuss the covalent character based on WBIs. In addition, Atoms-in-Molecules analysis was employed to locate the bond-critical points and to characterize the properties thereof. Regarding the cationic complexes, the calculations were also performed both with and without the $[BArF]^-$ counter anion (the latter are denoted as $\mathbf{1}^+$, $\mathbf{2}^+$ and $\mathbf{3}^+$) proving that the presence or absence of the anion has only negligible effect on the geometries, especially on the P → Sn bond distances (see Table S9), thus we will focus on the cations $\mathbf{1}^+$, $\mathbf{2}^+$ and $\mathbf{3}^+$.

Starting from the solid-state structures, we conducted conformational analysis searches for each of the compounds. After a set of low-energy isomers was located, the geometries were further optimized at the DFT level. Among the several isomers considered, the structures that were similar to those determined by sc-XRD were always proven to be the most stable. In most cases, it was possible to optimize geometries with three different bonding motifs, that is, 2, 1, or none of the phosphorus atoms establish dative bonds with the Sn centre, as unequivocally characterized by bond-critical points between the phosphorus and the tin centres. Moreover, in the case of complexes with no or one P → Sn dative bond, the spatial arrangement of the uncoordinated P centre was also tested, but we found that it only has a negligible influence on the stability of such complexes (with respect to the phenyl group, the in-plane position is more stable than the out-of-plane position). For more details and geometrical parameters, see the SI.

Comparison of possible rotamers

In the case of compound **1**, the rotamer lacking any P → Sn directional interaction has the lowest energy, while that exhibiting one bond is significantly less stable (13.6 kcal mol^{-1}; for details see Table S2). In this case, we were unable to optimize rotamers with two P → Sn contacts (all of the optimization runs resulted in the de-coordination of P atoms). For compounds **2** and **3**, all three possible rotamers characterized by 0, 1 or 2 P → Sn donations could be located, and these rotamers lie at similar energies (within ranges of 5.4 and 3.5 kcal mol^{-1} for **2** and **3**, respectively; see Tables S3 and S4). This observation indicates that the P → Sn interaction does not have a marked effect on the geometries and a strong stabilizing role. For comparison, a hypothetical complex that contains an $SnPh_3$ core connected to the aryl ring, was also investigated computationally. In this case, only the structure without any significant P → Sn interaction was found (see Table S5).

In contrast, cationic complexes $\mathbf{1}^+$–$\mathbf{3}^+$ differ markedly from neutral congeners. In these, the P → Sn interaction has a remarkable effect on the geometry and stability of the complexes. In all of the cases, both P centres establish interaction with the Sn centre. If one of the P → Sn interactions is absent, a significant destabilization is observable in terms of relative energy compared to the isomer with two P → Sn bonds (ΔE = 7.3/13.9/17.6 kcal mol^{-1}, for $\mathbf{1}^+/\mathbf{2}^+/\mathbf{3}^+$, respectively; see Tables S6–S8). This trend corresponds well with the finding that only one of the phosphorus atoms in $\mathbf{1}^+$ is blocked by borane leading to $\mathbf{[1(BH_3)]^+}$. Cleaving the second P → Sn bond results in very strained structures, which are highly destabilized with relative energies of ΔE = 39.5–61.4 kcal mol^{-1}, indicating the importance of the dative interactions for stabilization of the cations. However, in these geometries, a dative bond between the O and Sn centres forms in line with the high Lewis acidity of the tin centre (see the SI).

We also used relaxed scan calculations to screen the energy dependence upon changing the C_{ipso}–C_{ortho}–O–P dihedral angle. The rotation barrier is significantly lower in the neutral complexes (11.3–12.9 kcal mol^{-1}), than in their cationic counterparts (15.9–27.9 kcal mol^{-1}), in line with weaker P → Sn interactions in the former (Table S10).

In the following, we will discuss only the isomers having the lowest energies, which also resemble the solid-state structures.

Bonding analysis

The calculated geometrical parameters nicely agree with those obtained by the sc-X-ray diffraction measurements. The larger deviations (in a range of 0.053–0.133 Å) can be observed in the structures that exhibit the non-coordinated phosphorus centres, and the rotational flexibility of these arms leads to larger geometrical distortion. To understand the bonding patterns, it is straightforward to compare selected bonding parameters, namely the Wiberg Bond Indices (WBIs), the electron density (ρ) and the total energy density (H) in the P → Sn bond-critical points (BCPs). The WBIs reveal the covalent character of the bonds (without any reference), and their comparison is more straightforward than that of bond distance values. The electron density value at a bond-critical point describes the strength of the P → Sn interactions. As to differentiating between the nature of the interaction, the sign of H at the bond-critical point is negative in the case of stronger dative bonding, while positive for weaker non-covalent interactions (the values close to zero exclude a substantial covalent (dative) character). In the neutral complexes **1–3**, two different bonding situations can be distinguished. Weak, almost negligible, non-covalent interactions can be recognized for compounds **1** and **2** (Tables S2 and S3), which are illustrated by WBI values below 0.20 with practically zero H values. Based on these properties, this type of interaction resembles the so-called tetrel bond, which is a weak, element-specific, non-

covalent (σ-hole) interaction. However, due to steric crowding around the Sn centres, the P–Sn–Cl angle in these complexes deviates from linear, a common feature of σ-hole interactions. One of the phosphorus centres in **3** forms a stronger dative P → Sn interaction with WBI value 0.52 and quite negative *H* value of −0.017 (Table S4), which is in good agreement with the experimental sc-XRD structure. In stark contrast to the neutral analogues, in the cationic complexes $\mathbf{1}^+$–$\mathbf{3}^+$, two relatively strong P → Sn dative bonds stabilize the tin centre (Tables S6–S8). The substantial WBIs (in the range of 0.43–0.67) and the high electron density ρ values at the BCPs (from 0.048 to 0.073 e per Bohr^3) underline the strength and highly covalent character of these bonds, in line with the meaningful interaction energies described above.

To quantitatively assess the Lewis acidity of the Sn centre and the stabilization effects offered by the P → Sn interaction, the energy of the model complex formation reaction below (termed as interaction energy, ΔE_{int}) has been calculated for x = 0, 1, 2, 3 and 4, as well as for the mono-cationic counterparts (x = 0 to 3). The complex formation reactions utilizing the model phosphine (PhO)Ph_2P for obtaining the interaction energies ΔE_{int}:

$$(PhO)Ph_2P + SnPh_xCl_{4-x} \rightarrow (PhO)Ph_2P \rightarrow SnPh_xCl_{4-x}$$

$$(PhO)Ph_2P + [SnPh_xCl_{3-x}]^+ \rightarrow [(PhO)Ph_2P \rightarrow SnPh_xCl_{3-x}]^+$$

Importantly, these model reactions deliver the binding energy of a phosphorus centre to the tin acceptor in the absence of any geometrical constraints of the chelating backbone and thus describe the inherent strength of the P → Sn interaction in general. It should be mentioned that simpler phosphines such as PH_3 or PH_2(OMe) were also tested in addition to PPh_2(OPh); however, in most cases, the adducts with them underwent spontaneous dissociation during the optimisation runs. Nevertheless, the PPh_2(OPh) as a Lewis-base seems to be a realistic model for quantifying the strength of the P → Sn interactions (Table 2).

The computed reaction energies for complex formation show that in neutral complexes the formation of the P → Sn bond is somewhat exothermic, but endergonic. This is in line with the moderate strength of the P → Sn interactions and explains the small relative energy difference between the isomers and the high degree of conformational flexibility of the complexes. In the case of the $SnPh_3Cl$ and the $SnPh_4$, not even an adduct with P(Ph)$_2$(OPh) could be accessed (no minimum on the potential energy surface could be located), while for the other stannanes, the interaction energy is practically independent of the number of Cl and Ph centres (slightly decreases with the number of Cl centres). These results indicate that the interaction between the P and Sn centres is of a weak, non-covalent nature. In contrast to the neutral analogues, in the case of the cations $[SnPh_xCl_{3-x}]^+$ the forming P → Sn interactions effectively stabilize the complexes with significant reaction energies (−56.8 to −93.9 kcal mol^{-1}). These complex formation reactions gradually become more exothermic and exergonic with the number of Cl centres in the tin model cations, in line with the increasing Lewis acidity of these centres.

Analogous to the experiments mentioned above, we also obtained the borane affinities (ΔE_{BA}) of the complexes **1**–**3** and $\mathbf{1}^+$–$\mathbf{3}^+$ as the energy of their reactions with BH_3 leading to the corresponding borane adduct. Borane affinities indirectly quantify the strength of the P → Sn interaction (P → B bonds are expected to be similar in the formed adducts). The calculated interaction energies and borane affinities show a clear trend: the more negative the interaction energies (ΔE_{int}), the less prone the P centre is to cleavage of the P → Sn interaction and the less negative the borane affinity of the complex (Fig. 8 and Table S11). Again, the neutral complexes are rather similar to each other, their borane affinities are rather low (exothermic reactions), and the corresponding interaction energies are insignificant. This indicates a high tendency to cleave the P → Sn bond, which is in good agreement with the observation that all neutral congeners may capture one (**3**) or even two BH_3 Lewis acids. In contrast, in the case of cationic complexes, a monotonous increase in borane affinities can be observed in the direction $\mathbf{1}^+ \rightarrow \mathbf{2}^+ \rightarrow \mathbf{3}^+$. This means that changing the P → Sn bond to a P → B interaction becomes gradually more difficult in this direction. Nevertheless, the negative borane affinities corresponding to complexes $\mathbf{2}^+$ and $\mathbf{3}^+$ would suggest

Table 2 BSSE-corrected interaction energy and Gibbs free energy for the model compounds at the ωB97X-D/def2-TZVP//ωB97X-D/def2-SVP level of theory

	ΔE_{int} (kcal mol^{-1})	ΔG_{int} (kcal mol^{-1})
$SnCl_4$	−10.4	6.4
$SnPhCl_3$	−9.9	8.8
$SnPh_2Cl_2$	−9.8	9.0
$SnPh_3Cl$	—[a]	—[a]
$SnPh_4$	—[a]	—[a]
$SnCl_3^+$	−92.7	−75.5
$SnPhCl_2^+$	−73.6	−56.3
$SnPh_2Cl^+$	−57.9	−39.7
$SnPh_3^+$	−55.8	−36.2

[a] No adducts could be optimized due to spontaneous dissociation.

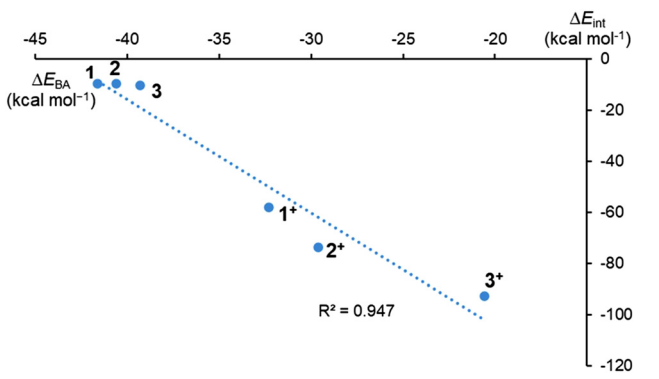

Fig. 8 BSSE-corrected interaction energy and borane affinity values calculated at the ωB97X-D/def2-TZVP//ωB97X-D/def2-SVP level of theory.

that the attack of the borane is thermodynamically feasible. However, the activation barrier to cleave the P → Sn bond is large for these complexes (23.3 and 27.9 kcal mol^{-1}, respectively, unlike the other cases) and thus, borane addition is kinetically hampered. This observation is in agreement with the outcome of the experiments, in that **[1(BH$_3$)]$^+$** could only be obtained by coordination of one molecule of borane to **1$^+$**. In general, the Lewis acidity of the tin centre decreases with the increasing number of the phenyl groups (while the steric crowding increases), leading to the weakening of the P → Sn interaction.

Finally, to further supplement the observations from the heteronuclear NMR experiments, we simulated the ^{31}P and ^{119}Sn chemical shifts in these complexes (Tables S12 and S13). Nuclear shielding parameters were calculated considering the scalar and spin–orbit effects. In the case of ^{119}Sn chemical shifts the standard is $SnMe_4$ ($\delta_{ref}(^{119}Sn)$ = 0 ppm), while for the ^{31}P chemical shifts **ArBr** employed in the experiments was chosen ($\delta_{ref}(^{31}P)$ = 154.2 ppm). The latter was selected, as PH_3, which is typically applied as standard in DFT computations, was found to be a less suitable reference due to the complexity of the P,C,P-chelate complexes and the strongly differing chemical environment. As the NMR spectra were recorded in non-coordinating and lower polarity solvents (C_6D_6, CD_2Cl_2 and $CDCl_3$), the data values calculated without solvation models show good agreement with the experimental ones. In general, the calculated ^{31}P and ^{119}Sn chemical shifts show excellent correlation with the experimental data (R^2 = 0.989, see Fig. S90). However, for the latter, a precise description of the spin–orbit coupling is required (R^2 = 0.979, see Fig. S91).

The ^{119}Sn NMR chemical shifts and $^1J(^{119}Sn,^{31}P)$ coupling constants are also practical indicators for elucidating the geometries of organotin compounds, especially with regard to the coordination sphere around the tin centres. In complexes **1** and **2**, the ^{119}Sn NMR shifts reveal four-coordinated tin centres, in line with the singlet resonances lacking any visible $^1J(^{119}Sn,^{31}P)$ coupling in the experimental spectra. In contrast, the significantly more shielded tin centre in complex **3** signifies a hypervalent tin centre. Based on the computationally obtained geometries, a penta-coordinated or a hexa-coordinated (with four stronger and two weaker donations) motif seems possible. The former is consistent with the geometries obtained by sc-XRD. In the case of the cationic complexes **1$^+$**–**3$^+$**, the signals are considerably shifted up-field, indicating structures with penta-coordinated tin centers, stabilized by two strong P → Sn interactions. A further trend can be observed in the ^{31}P NMR chemical shifts corresponding to the coordinated P centres, which are more shielded compared to **ArBr**. In cationic complexes, with an increasing number of chlorine substituents at the Sn centre, the ^{31}P NMR chemical shifts gradually decrease (105.7/97.2/86.2 ppm). This is in good agreement with the intensification of Lewis acidity of the Sn centres exemplified by the complex formation reaction energies (−37.2/−43.7/−57.4 kcal mol^{-1}) and with the increase of WBI indices (0.45/0.51/0.54). The lower ^{31}P NMR chemical shifts indicate a stronger dative bond, with a higher covalency triggered by the more Lewis acidic tin centre.

In general, the trend of the calculated $^1J(^{119}Sn,^{31}P)$ coupling constants follows that of the experimentally obtained values (see Table 1). In certain cases, the numerical agreement is excellent, whereas for several compounds, significant deviations can be found. The estimation of $^1J(^{119}Sn,^{31}P)$ values is especially challenging due to the presence of the heavy element. It should be noted that the coupling constants are in general strongly influenced by minor changes in geometrical parameters (see Fig. S92–S94), often resulting in substantial deviations between the experimental and calculated values.[29] Indeed, the coupling constant shows a strong dependency on the Sn–P distance and dihedral angles (see Fig. S95 and S96).

Conclusions

A whole set of organotin(IV) complexes bearing the P,C,P-ligand was synthesized and characterized, representing the first utilization of a classical mono-anionic phosphorus-based ligand in the p-block of the periodic system. The ligand exhibited remarkable coordination flexibility and variability depending on the Lewis acidity of the tin centre and resulted in three basic bonding types. The ligand can serve as a pure monodentate C-anionic ligand with two pendant phosphorus atoms, while these donors are readily available for donation to metal ions as exemplified in complexes **4·AgOTf** and **4·AgSbF$_6$**, which is promising for the synthesis of related bimetallic complexes in the future. In compounds containing the more Lewis acidic tin atom, a C,P-chelate or a tridentate P,C,P-pincer coordination with two strong P → Sn interactions could be established. It should be noted that this ligand framework allowed the isolation of a highly Lewis acidic dichlorotin(IV) cation **3$^+$** and four-coordinated cation **[1(BH$_3$)]$^+$**, which had not been achieved before for the related N,C,N- or O,C,O-pincer ligands. The DFT calculations on these compounds support the high flexibility of the coordination environment. The neutral analogues may adopt several rotamers that have similar relative energies and the P → Sn bonding can be described as weakly non-covalent interactions, similar to tetrel bonds. In contrast, the cationic counterparts are characterized by stronger dative P → Sn bonds. The strength of this interaction is primarily governed by the Lewis acidity of the Sn(IV) center.

Owing to the fact that p-block complexes with O,C,O-, but especially N,C,N-pincer ligands,[4,10,13] have for a long time been among the most successful, interesting, and continuously explored main group compounds, the introduction of totally unexplored heavier P,C,P-analogues is, in our opinion, a highly desirable step forward in this field. This work should help in this effort, and exciting developments in this direction are envisaged in the near future.

Conflicts of interest

There are no conflicts to declare.

Data availability

The data supporting this article including syntheses details, NMR, IR spectra, details for crystallography and theoretical studies have been included as part of the SI. Supplementary information is available. See DOI: **https://doi.org/10.1039/d5dt01873k**.

CCDC 2469044 (**2**), 2469048 (**3**), 2469047 (**4·AgOTf**), 2469052 (**4·AgSbF$_6$**), 2469053 (**1[BArF]**), 2469049 (**3[BArF]**), 2469051 (**1(BH$_3$)$_2$**), 2469046 (**2(BH$_3$)$_2$**), 2469050 (**[1(BH$_3$)][BArF]**) and 2469045 (**ArBr(BH$_3$)$_2$**) contain the supplementary crystallographic data for this paper.[30a–j]

Acknowledgements

The computations presented here were conducted by the IT4Innovations National Supercomputing Center under the program of the Ministry of Education, Youth and Sports of the Czech Republic through the e-INFRA CZ(ID:90254) – project OPEN-31-21, Computational investigation on the reactivity of complexes containing group 15 elements. We acknowledge the Digital Government Development and Project Management Ltd for awarding us access to the Komondor HPC facility based in Hungary. This work is supported by the K-147095 and TKP-2021-BME-NVA02 offered by NKFIH, EKÖP-24-3-BME-231 and DKÖP-23-1-BME-29 of NKFIH and of BME-VBK and the Michael Somogyi program of BME-VBK. We thank the referees for their valuable comments that helped to improve this manuscript considerably.

References

1 (*a*) C. J. Moulton and B. L. Shaw, *J. Chem. Soc., Dalton Trans.*, 1976, 1020; (*b*) C. S. Creaser and K. W. Kaska, *Inorg. Chim. Acta*, 1978, **30**, L325; (*c*) G. van Koten, K. Timmer, J. G. Noltes and A. L. Spek, *J. Chem. Soc., Chem. Commun.*, 1978, 250.

2 There is a wide variety of pincer complexes known in literature; in this introduction we consider only the classical C-monoanionic ones directly and closely related to this work.(*a*) *The chemistry of pincer compounds*, ed. D. Morales-Morales and C. M. Jensen, Elsevier, Amsterdam, 2007; (*b*) Pincer compounds, in *Chemistry and Applications*, ed. D. Morales-Morales, Elsevier, Amsterdam, 2018; (*c*) Special Collection, in *Eur. J. Inorg. Chem.*, ed. G. Van Koten, D. Morales-Morales and K. Hollis, Articles at Pincer Chemistry and Catalysis: European Journal of Inorganic Chemistry – Chemistry Europe (wiley.com), 2020; (*d*) H. Valdés, J. M. Germán-Acacio, G. van Koten and D. Morales-Morales, *Dalton Trans.*, 2022, **51**, 1724; (*e*) A. Murkherjee and D. Milstein, *ACS Catal.*, 2018, **8**, 11435.

3 For selected reviews devoted to P,C,P-ligands see: (*a*) W. Leis, H. A. Mayer and W. C. Kaska, *Coord. Chem. Rev.*, 2008, **252**, 1787; (*b*) J. M. Serrano-Becerra and D. Morales-Morales, *Curr. Org. Synth.*, 2009, **6**, 169; (*c*) R. A. Manzano and R. D. Young, *Coord. Chem. Rev.*, 2021, **449**, 214215; (*d*) Y. Wang, Z. Huang, G. Liu and Z. Huang, *Acc. Chem. Res.*, 2022, **55**, 2148; (*e*) L. Boisvert and K. I. Goldberg, *Acc. Chem. Res.*, 2012, **45**, 899.

4 (*a*) R. Jambor and L. Dostál, Chapter 16, in *The chemistry of pincer compounds*, ed. D. Morales-Morales and C. M. Jensen, Elsevier, Amsterdam, 2007, ISBN: 978-0-444-53138-4; (*b*) R. Jambor and L. Dostál, *Top. Organomet. Chem.*, 2013, **40**, 175; (*c*) L. Dostál, R. Jambor and D. Morales-Morales, Chapter 3, in *Pincer compounds. Chemistry and Applications*, Elsevier, Amsterdam, 2018. ISBN: 978-0-12-812931-9; (*d*) L. Dostál, R. Jambor, M. Aman and M. Hejda, *ChemPlusChem*, 2020, **85**, 2320.

5 J. T. B. H. Jastrzebski, P. A. van der Schaaf, J. Boersma, G. van Koten, M. C. Zoutberg and D. Heijdenrijk, *Organometallics*, 1989, **8**, 1373.

6 M. Mehring, M. Schürmann and K. Jurkschat, *Organometallics*, 1998, **17**, 1227.

7 R. Jambor, L. Dostál, A. Růžička, I. Císařová, J. Brus, M. Holčapek and J. Holeček, *Organometallics*, 2002, **21**, 3996.

8 (*a*) M. El Ezzi, R. Lenk, D. Madec, J. M. Sotiropoulos, S. Mallet-Ladeira and A. Castel, *Angew. Chem., Int. Ed.*, 2015, **54**, 805; (*b*) M. Deak, P. M. Petrar, S. Mallet-Ladeira, L. Silaghi-Dumistrescu, G. Nemes and D. Madec, *Chem. – Eur. J.*, 2016, 1349.

9 Several examples for N,C,N-ligands: (*a*) A. Caise, L. P. Griffin, A. Heilmann, C. McManus, J. Campos and S. Aldridge, *Angew. Chem., Int. Ed.*, 2021, **60**, e202104643; (*b*) A. Caise, L. P. Griffin, C. McManus, A. Heilmann and S. Aldridge, *Angew. Chem., Int. Ed.*, 2022, **61**, e2021174; (*c*) A. Caise, J. Hicks, A. Heilmann and S. Aldridge, *Chem. Commun.*, 2023, **59**, 7251; (*d*) R. Jambor, B. Kašná, K. N. Kirschner, M. Schürmann and K. Jurkschat, *Angew. Chem., Int. Ed.*, 2008, **47**, 1650; (*e*) M. Bouška, L. Dostál, Z. Padělková, A. Lyčka, S. Herres-Pawlis and R. Jambor, *Angew. Chem., Int. Ed.*, 2012, **51**, 3477; (*f*) A. Caise, A. E. Crumpton, P. Vasko, J. Hicks, C. McManus, N. H. Rees and S. Aldridge, *Angew. Chem., Int. Ed.*, 2022, **61**, e202114926; (*g*) S. P. Chia, H. W. Xi, Y. Li, K. H. Lim and C. W. So, *Angew. Chem., Int. Ed.*, 2013, **52**, 6298; (*h*) S. Khan, R. Michel, J. M. Dieterich, R. A. Mata, H. W. Roesky, J. P. Demers, A. Lange and D. Stalke, *J. Am. Chem. Soc.*, 2011, **133**, 17889; (*i*) S. P. Chia, R. Ganguly, Y. Li and C. W. So, *Organometallics*, 2012, **31**, 2012; (*j*) S. Khan, P. P. Samuel, R. Michel, J. M. Dieterich, R. A. Mata, J. P. Demers, A. Lange, H. W. Roesky and D. Stalke, *Chem. Commun.*, 2012, **48**, 4890; (*k*) S. P. Chia, E. Carter, H. W. Xi, Y. Li and C. W. So, *Angew. Chem., Int. Ed.*, 2014, **53**, 8455; (*l*) A. Růžička, L. Dostál, R. Jambor, V. Buchta, J. Brus, I. Císařová, M. Holčapek and J. Holeček, *Appl. Organomet. Chem.*, 2002, **16**, 315; (*m*) P. Novák, I. Císařová, L. Kolářová, A. Růžička and J. Holeček, *J. Organomet. Chem.*, 2007, **692**, 4287.

10 For O,C,O-ligands: (*a*) B. Kašná, R. Jambor, L. Dostál, I. Císařová, J. Holeček and B. Štíbr, *Organometallics*, 2006,

25, 5139; (*b*) B. Kašná, R. Jambor, L. Dostál, A. Růžička, I. Císařová and J. Holeček, *Organometallics*, 2004, **23**, 5300; (*c*) M. Wagner, C. Dietz, S. Krabbe, S. G. Koller, C. Strohmann and K. Jurkschat, *Inorg. Chem.*, 2012, **51**, 6851; (*d*) M. Wagner, V. Deaky, C. Dietz, J. Martincová, B. Mahieu, R. Jambor, S. HerrePawlis and K. Jurkschat, *Chem. – Eur. J.*, 2013, **19**, 6695; (*e*) M. Wagner, T. Zoller, W. Hiller, M. H. Prosenc and K. Jurkschat, *Chem. – Eur. J.*, 2013, **19**, 9463; (*f*) K. Jurkschat, K. Peveling and M. Schurmann, *Eur. J. Inorg. Chem.*, 2003, 3563.

11 Several examples for N,C,N-ligands: (*a*) G. G. Briand, T. George, G. A. MacNeil, J. D. Masuda, B. J. MacLean, M. W. R. Mosher, G. M. Sandala, P. Srinivasan, A. H. Stockli, R. L. Vanderkloet and C. J. Walsby, *Eur. J. Inorg. Chem.*, 2023, **26**, e2022005; (*b*) T. Řičica, Y. Milasheuskaya, Z. Růžičková, P. Němec, P. Švanda, Z. O. Zmrhalová, R. Jambor and M. Bouška, *Chem. – Asian J.*, 2019, **14**, 4229; (*c*) V. Lomeli, B. G. McBurnett and A. H. Cowley, *J. Organomet. Chem.*, 1998, **562**, 123; (*d*) A. H. Cowley, F. P. Gabbai, D. A. Atwood, C. J. Carrano, L. M. Mokry and M. R. Bond, *J. Am. Chem. Soc.*, 1994, **116**, 1559; (*e*) T. Řičica, L. Dostál, Z. Růžičková, L. Beneš, P. Němec, M. Bouška, J. M. Macák, P. Knotek, P. Ruleová and R. Jambor, *Chem. – Eur. J.*, 2018, **24**, 14470; (*f*) A. H. Cowley, R. A. Jones, M. A. Mardones, J. Ruiz, J. L. Atwood and S. G. Bott, *Angew. Chem., Int. Ed. Engl.*, 1990, **29**, 1150; (*g*) T. Řičica, T. Světlík, L. Dostál, A. Růžička, K. Růžička, L. Beneš, P. Němec, M. Bouška and R. Jambor, *Chem. – Eur. J.*, 2016, **22**, 18817; (*h*) C. Cui, H. W. Roesky, M. Noltemeyer and H. G. Schmidt, *Inorg. Chem.*, 2000, **39**, 3678; (*i*) M. Saito, K. Matsumoto, M. Fujita and M. Minoura, *Heteroat. Chem.*, 2014, **25**, 354; (*j*) Z. Liu, R. Ganguly and D. Vidovic, *Dalton Trans.*, 2017, **46**, 753; (*k*) T. Iwase, A. Habibzadeh, C. Goonesinghe, K. Nyamayro, J. Chang, J. W. L. Poon, S. H. Rushdy, J. Koh, B. O. Patrick and P. Mehrkhodavandi, *Dalton Trans.*, 2024, **53**, 19337.

12 For O,C,O-ligands: (*a*) L. Dostál, R. Jambor, A. Růžička, I. Císařová and J. Holeček, *Appl. Organomet. Chem.*, 2005, **19**, 797; (*b*) S. J. Cassidy, I. Brettell-Adams, L. E. McNamara, M. F. Smith, M. Bautista, H. Cao, M. Vasiliu, D. L. Gerlach, F. Qu, N. I. Hammer, D. A. Dixon and P. A. Rupar, *Organometallics*, 2018, **37**, 3732.

13 Several examples for N,C,N-ligands: (*a*) D. A. Atwood, A. H. Cowley and J. Ruiz, *Inorg. Chim. Acta*, 1992, **198**, 271; (*b*) L. Dostál, R. Jambor, A. Růžička and J. Holeček, *Organometallics*, 2008, **27**, 2169; (*c*) G. Strimb, A. Pollnitz, C. I. Rat and C. Silvestru, *Dalton Trans.*, 2015, **44**, 9927; (*d*) G. Dunes, A. P. Soran and C. Silvestru, *Dalton Trans.*, 2022, **51**, 10406; (*e*) P. Novák, M. Erben, R. Jambor, M. Hejda, A. Růžička, E. Rychagovam, S. Ketkov and L. Dostál, *Dalton Trans.*, 2023, **52**, 218; (*f*) H. J. Breunig, M. G. Nema, C. Silvestru, A. P. Soran and C. Varga, *Dalton Trans.*, 2010, **39**, 11277; (*g*) I. J. Casely, J. W. Ziller, M. Fang, F. Furche and W. J. Evans, *J. Am. Chem. Soc.*, 2011, **133**, 5244; (*h*) M. Hejda, R. Jirásko, A. Růžička, R. Jambor and L. Dostál, *Organometallics*, 2020, **39**, 4320; (*i*) L. Balazs, H. J. Breunig, E. Lork, A. Soran and C. Silvestru, *Inorg. Chem.*, 2006, **45**, 2341; (*j*) A. P. Soran, C. Silvestru, H. J. Breunig, G. Balazs and J. C. Green, *Organometallics*, 2007, **26**, 1196; (*k*) D. R. Kindra, I. J. Casely, M. E. Fieser, J. W. Ziller, F. Furche and W. J. Evans, *J. Am. Chem. Soc.*, 2013, **135**, 7777; (*l*) P. Šimon, F. De Proft, R. Jambor, A. Růžička and L. Dostál, *Angew. Chem., Int. Ed.*, 2010, **49**, 5468; (*m*) M. Hejda, R. Jirásko, A. Růžička, R. Jambor and L. Dostál, *Organometallics*, 2020, **39**, 4320; (*n*) X. Yang, E. J. Reijerse, N. Nothling, D. J. SantaLucia, M. Leutzsch, A. Schnegg and J. Cornella, *J. Am. Chem. Soc.*, 2023, **145**, 5618; (*o*) T. Tsuruta, D. Spinnato, H. W. Moon, M. Leutzsch and J. Cornella, *J. Am. Chem. Soc.*, 2023, **145**, 25538; (*p*) H. W. Moon, F. Wang, K. Bhattacharyya, O. Planas, M. Leutzsch, N. Nothling, A. A. Auer and J. Cornella, *Angew. Chem., Int. Ed.*, 2023, **62**, e202313578; (*q*) H. W. Moon and J. Cornella, *ACS Catal.*, 2022, **12**, 1382 and references cited therein. (*r*) M. Huang, K. Li, Z. Zhang and J. Zhou, *J. Am. Chem. Soc.*, 2024, **146**, 20432; (*s*) I. Vránová, M. Alonso, R. Jambor, A. Růžička, J. Turek and L. Dostál, *Chem. – Eur. J.*, 2017, **23**, 2340; (*t*) I. Vránová, V. Kremláček, M. Erben, J. Turek, R. Jambor, A. Růžička, M. Alonso and L. Dostál, *Dalton Trans.*, 2017, **46**, 3556; (*u*) M. T. Nguyen, B. Babidullin and G. I. Nikonov, *Dalton Trans.*, 2018, **47**, 17011.

14 For O,C,O-ligands: (*a*) K. Peveling, M. Schurmann, S. Herres-Pawlis, C. Silvestru and K. Jurkschat, *Organometallics*, 2011, **30**, 5181; (*b*) L. Dostál, I. Císařová, R. Jambor, R. Jirásko and J. Holeček, *Organometallics*, 2006, **25**, 4366; (*c*) L. Dostál, P. Novák, R. Jambor, A. Růžička, I. Císařová, R. Jirásko and J. Holeček, *Organometallics*, 2007, **26**, 2911; (*d*) M. Chovancová, R. Jambor, A. Růžička, R. Jirásko, I. Císařová and L. Dostál, *Organometallics*, 2009, **28**, 1934.

15 For N,C,O-ligands: (*a*) L. Dostál, R. Jambor, A. Růžička, R. Jirásko, J. Holeček and F. De Proft, *Dalton Trans.*, 2011, **40**, 8922; (*b*) J. Vrána, R. Jambor, A. Růžička, A. Lyčka and L. Dostál, *J. Organomet. Chem.*, 2012, **718**, 40.

16 Examples for all ligands: (*a*) M. Hejda, L. Doležal, J. Blahut, E. Hupf, J. Tydlitát, R. Jambor, A. Růžička, J. Beckmann and L. Dostál, *Dalton Trans.*, 2023, **52**, 16235; (*b*) A. K. Gupta, R. Deka, H. B. Singh and R. J. Butcher, *New J. Chem.*, 2019, **43**, 13225; (*c*) R. Deka, A. Gupta, A. Sarkar, R. J. Butcher and H. B. Singh, *Eur. J. Inorg. Chem.*, 2020, 4170; (*d*) A. Beleaga, V. R. Bojan, A. Pollinitz, C. I. Rat and C. Silvestru, *Dalton Trans.*, 2011, **40**, 8830; (*e*) A. Gupta, R. Deka, S. Raju, H. B. Singh and R. J. Butcher, *J. Organomet. Chem.*, 2019, **894**, 10; (*f*) A. Pop and A. Silvestru, *Polyhedron*, 2019, **160**, 279; (*g*) A. Pop, A. Silvestru, E. J. Juarez-Perez, V. Lippolis and C. Silvestru, *Dalton Trans.*, 2014, **43**, 2221; (*h*) H. Fujihara, H. Nima and N. Furukawa, *J. Am. Chem. Soc.*, 1995, **117**, 10153; (*i*) R. Deziel, S. Goulet, L. Grenier, J. Bordeleau and J. Bernier, *J. Org. Chem.*, 1993, **58**, 3619; (*j*) K. Okamoto, Y. Nishibayashi, S. Uemura and A. Toshimitsu, *Angew. Chem., Int. Ed.*, 2005, **44**, 3588; (*k*) S. S. Zade, S. Panda,

H. B. Singh, R. B. Sunoj and R. J. Butcher, *J. Org. Chem.*, 2005, **70**, 3693.

17 For a few examples see: (*a*) A. V. Plukeev, S. C. Capelli and O. F. Wendt, *Chem. Sci.*, 2023, **14**, 12308; (*b*) M. Montag, I. Efremenko, R. Cohen, L. J. W. Shimon, G. Leitus, Y. Diskin-Posner, Y. Ben-David, H. Salem, J. M. L. Martin and D. Milstein, *Chem. – Eur. J.*, 2010, **16**, 328; (*c*) U. S. D. Paul, H. Braunschweig and U. Radius, *Chem. Commun.*, 2016, **52**, 8573; (*d*) T. J. Hebden, A. J. St John, D. G. Gusev, W. Kaminsky, K. I. Goldberg and M. Heinekey, *Angew. Chem., Int. Ed.*, 2010, **50**, 1873; (*e*) J. Song, Q. Liao, X. Hong, L. Jin and N. Mézailles, *Angew. Chem., Int. Ed.*, 2021, **60**, 12242; (*f*) A. Cartwright Sykes, P. White and M. Brookhart, *Organometallics*, 2006, **25**, 1664; (*g*) D. Himmelbauer, B. Stoger, L. F. Veiros, M. Pignitter and K. Kirchner, *Organometallics*, 2019, **38**, 4669; (*h*) N. Hidalgo, J. J. Moreno, I. García-Rubio and J. Campos, *Angew. Chem., Int. Ed.*, 2022, **61**, e202206831; (*i*) W. Huang, L. Y. Peng, J. Zhang, C. Liu, G. Song, J. H. Su, W. H. Fang, G. Cui and S. Hu, *J. Am. Chem. Soc.*, 2023, **145**, 811; (*j*) S. Ramakrishnan, S. Chakraborty, W. W. Brennessel, C. E. D. Chidsey and W. D. Jones, *Chem. Sci.*, 2016, **7**, 117; (*k*) M. C. Denney, V. Pons, T. J. Hebden, D. M. Heinekey and K. I. Goldberg, *J. Am. Chem. Soc.*, 2006, **128**, 12048; (*l*) J. Hu, Q. J. Bruch and A. J. M. Miller, *J. Am. Chem. Soc.*, 2021, **143**, 945; (*m*) J. Zhang, W. Huang, K. Han, G. Song and S. Hu, *Dalton Trans.*, 2022, **51**, 12250.

18 L. Webster, T. Kramer and F. M. Chadwick, *Dalton Trans.*, 2022, **51**, 16714.

19 A. G. Davies, P. G. Harrison, J. D. Kennedy, T. N. Mitchell, R. J. Puddenphatt and W. McFarlane, *J. Chem. Soc. C*, 1969, 1136.

20 P. Pyykkö and M. Atsumi, *Chem. – Eur. J.*, 2009, **15**, 186.

21 A. W. Addison, T. N. Rao, J. Reedijk, J. van Rijn and G. C. Verschoor, *J. Chem. Soc., Dalton Trans.*, 1984, 1349.

22 R. Jambor, I. Císařová, A. Růžička and J. Holeček, *Acta Crystallogr., Sect. C:Cryst. Struct. Commun.*, 2001, **57**, 373.

23 A. Růžička, R. Jambor, J. Brus, I. Císařová and J. Holeček, *Inorg. Chim. Acta*, 2001, **323**, 163.

24 M. Mehring, C. Löw, M. Schurmann and K. Jurkschat, *Eur. J. Inorg. Chem.*, 1999, 887.

25 E. MacDonald, L. Doyle, N. Burford, U. Werner-Zwanziger and A. Decken, *Angew. Chem., Int. Ed.*, 2011, **50**, 11474.

26 V. K. Greenacre, R. P. King, W. Levason and G. Reid, *Dalton Trans.*, 2019, **48**, 17097.

27 K. Peveling, M. Henn, C. Löw, M. Mehring, M. Schurmann, B. Costisella and K. Jurkschat, *Organometallics*, 2004, **23**, 1501.

28 (*a*) J. Zechovský, E. Kertész, V. Kremláček, M. Hejda, T. Mikysek, M. Erben, A. Růžička, R. Jambor, Z. Benkő and L. Dostál, *Organometallics*, 2022, **41**, 2535; (*b*) V. Kremláček, E. Kertész, M. Erben, A. Růžička, R. Jambor, Z. Benkő and L. Dostál, *Chem. – Eur. J.*, 2025, **31**, e202404751; (*c*) J. Zechovský, E. Kertész, M. Erben, M. Hejda, R. Jambor, A. Růžička, Z. Benkő and L. Dostál, *ChemPlusChem*, 2024, **89**, e202300573; (*d*) J. Zechovský, E. Kertész, M. Erben, R. Jambor, A. Růžička, Z. Benkő and L. Dostál, *ChemPlusChem*, 2023, **88**, e202300018.

29 (*a*) A. Bagno, G. Casella and G. Saielli, *J. Chem. Theory Comput.*, 2006, **2**, 37; (*b*) J. Arras, K. Eichele, B. Maryasin, H. Schubert, C. Ochsenfeld and L. Wesemann, *Inorg. Chem.*, 2016, **55**(9), 4669; (*c*) R. Mokrai, J. Barrett, D. C. Apperley, A. S. Batsanov, Z. Benkő and D. Heift, *Chem. – Eur. J.*, 2019, **25**, 4017; (*d*) R. Mokrai, J. Barrett, D. C. Apperley, Z. Benkő and D. Heift, *Inorg. Chem.*, 2020, **59**, 8916.

30 (*a*) R. Chlebík, E. Kertész, M. Erben, A. Růžička, R. Jambor, Z. Benkő and L. Dostál, CCDC 2469044: Experimental Crystal Structure Determination, 2025, DOI: **10.5517/ccdc.csd.cc2nw7ld**; (*b*) R. Chlebík, E. Kertész, M. Erben, A. Růžička, R. Jambor, Z. Benkő and L. Dostál, CCDC 2469045: Experimental Crystal Structure Determination, 2025, DOI: **10.5517/ccdc.csd.cc2nw7mf**; (*c*) R. Chlebík, E. Kertész, M. Erben, A. Růžička, R. Jambor, Z. Benkő and L. Dostál, CCDC 2469046: Experimental Crystal Structure Determination, 2025, DOI: **10.5517/ccdc.csd.cc2nw7ng**; (*d*) R. Chlebík, E. Kertész, M. Erben, A. Růžička, R. Jambor, Z. Benkő and L. Dostál, CCDC 2469047: Experimental Crystal Structure Determination, 2025, DOI: **10.5517/ccdc.csd.cc2nw7ph**; (*e*) R. Chlebík, E. Kertész, M. Erben, A. Růžička, R. Jambor, Z. Benkő and L. Dostál, CCDC 2469048: Experimental Crystal Structure Determination, 2025, DOI: **10.5517/ccdc.csd.cc2nw7qj**; (*f*) R. Chlebík, E. Kertész, M. Erben, A. Růžička, R. Jambor, Z. Benkő and L. Dostál, CCDC 2469049: Experimental Crystal Structure Determination, 2025, DOI: **10.5517/ccdc.csd.cc2nw7rk**; (*g*) R. Chlebík, E. Kertész, M. Erben, A. Růžička, R. Jambor, Z. Benkő and L. Dostál, CCDC 2469050: Experimental Crystal Structure Determination, 2025, DOI: **10.5517/ccdc.csd.cc2nw7sl**; (*h*) R. Chlebík, E. Kertész, M. Erben, A. Růžička, R. Jambor, Z. Benkő and L. Dostál, CCDC 2469051: Experimental Crystal Structure Determination, 2025, DOI: **10.5517/ccdc.csd.cc2nw7tm**; (*i*) R. Chlebík, E. Kertész, M. Erben, A. Růžička, R. Jambor, Z. Benkő and L. Dostál, CCDC 2469052: Experimental Crystal Structure Determination, 2025, DOI: **10.5517/ccdc.csd.cc2nw7vn**; (*j*) R. Chlebík, E. Kertész, M. Erben, A. Růžička, R. Jambor, Z. Benkő and L. Dostál, CCDC 2469053: Experimental Crystal Structure Determination, 2025, DOI: **10.5517/ccdc.csd.cc2nw7wp**.